

Article

Application of mathematical search algorithms for unknown material properties in Additive Manufacturing simulations

Aaron Flood ^{1,†,*}, Rachel Boillat ^{1,†,‡}, Sriram Isanaka ^{2,†,‡} and Frank Liou ^{3,†,‡}

¹ Affiliation 1; rmb8t6@umsystem.edu

² Affiliation 2; sihyd@umsystem.edu

³ Affiliation 3; liou@umsystem.edu

* Correspondence: ajfrk6@umsystem.edu

† These authors contributed equally to this work.

‡ Current address: Missouri University of Science and Technology; Department of Mechanical and Aerospace Engineering, 194 Toomey Hall, Rolla, MO 65409, United States

Abstract: Additive manufacturing (AM) simulations have risen as a way to better understand the effect of processing parameters on builds. They are effective for materials which are well characterized and published, however for newer or proprietary materials, they cannot provide accurate results due to the lack of knowledge of material properties. This work demonstrates the process of the application of mathematical search algorithms to develop an optimized material dataset which results in accurate simulations. This was done with 7000 series aluminum and the laser directed energy deposition (DED) process. The Nelder-Mead search algorithm was able to develop an optimized dataset which had a combined width and depth error of just 9.1%. This optimization started from a generic aluminum material properties dataset found in the literature which had an initial error of 600%.

Keywords: Additive manufacturing (AM), Mathematical modeling, Mathematical search, Material properties, Aluminum

1. Introduction

Additive manufacturing (AM) is an emerging manufacturing technique which has the potential to revolutionize manufacturing. To realize this revolution, it is necessary to be able to produce components reliably and to understand the process well enough to ensure that builds are consistent enough that the performance of the completed build can be guaranteed. To do this, researchers and manufacturers have turned to mathematical modeling to understand the process [1].

The differences in simulation techniques can vary based on the desired response from the simulation and the underlying assumptions which were made during the development of the models. One example of this can be seen when comparing the mathematical models presented in [1], [2], and [3]. They all attempt to model roughly the same aspect of the build but take very different approaches. [1] take a purely physics-based approach to the solution and works from first principle of the physical process being modeled. On the contrary, [2] is a data driven model which used a breadth of data to develop a mathematical model which properly predicts the material behavior. In between these models exists [3] which attempts to marry the two approaches and develop a physics-based model that uses data to improve accuracy. The one unifying characteristic of these, and all, mathematical models, is the need for the inclusion of a dataset which defines the behavior of the material being investigated, this is colloquially referred to as the material properties. These material properties can vary in literature and this variance in values can lead to a discrepancy in simulation results [4].

Though variation exists in the literature, values can be found and used when the material is well characterized and published. An example of a well published material

Citation: Flood, A.; Boillat, R.; Isanaka, S.; Liou, F. Application of mathematical search algorithms for unknown material properties in Additive Manufacturing simulations. *Metals* **2023**, *1*, 0. <https://doi.org/>

Received:

Revised:

Accepted:

Published:

Copyright: © 2023 by the authors. Submitted to *Metals* for possible open access publication under the terms and conditions of the Creative Commons Attribution (CC BY) license (<https://creativecommons.org/licenses/by/4.0/>).

is Ti-64 where it is easy to find literature which reports the material properties such as in [5], [6], and [7]. However, for materials which are not well understood and published, such as specific aluminum alloys, it can be very challenging though possible to find some properties such as [8] and [9]. There is a need to determine a complete dataset of the material properties, or at a minimum, develop the dataset which produces the most accurate simulation results. This can be accomplished by expending the necessary resources to measure the needed properties using advanced equipment. This process can be expensive and time-consuming which has led to the development of material simulations which attempt to predict the material properties, such as [10]. Though faster and cheaper than experimental results, they, like all simulations, have an error that is associated with them. Using these values alone can lead to unknown errors stacking up in the AM models. This problem also applies to materials where the tolerances for alloying elements is so wide that specimen of the same alloy can have different material properties.

In order to develop a dataset which produces accurate AM simulation results, a multi-objective optimization scheme can be used as a search algorithm to determine the dataset which produces the most realistic results. This can be used to develop a dataset for a new alloy along with for a specific batch of stock which has been procured from a supplier.

This work will aim to address one of the current desires in metal AM which is to be able to produce parts out of aluminum. The desire is evident by the volume of effort being applied to aluminum AM ([11], [12], [13]). The challenge associated with this stems from the wide range of alloys which have wildly varying material properties and are not well published. One of the weldable high-strength alloys which has been targeted for metal AM is 7050 [14]. Though the material is widely available, temperature-dependent material properties are not readily available. Therefore, this work will find material properties in literature which are an approximation of the 7050 aluminum, namely sister alloys with similar compositions, as a starting point for the search algorithm. From that starting database, a search algorithm will be applied to develop a material dataset which produces more accurate AM simulation results.

2. Materials and Methods

2.1. Simulation description

The model used in this study was developed at Missouri University of Science and Technology. This simulation has the express goal of being efficient while still holding true to physics models. In order to accomplish this, it heavily leverages GPU processing by utilizing image processing techniques. The simulation was developed with the laser DED processes in mind, however, it was developed in a modular manner such that it can be applied to most AM processes.

The model is a voxel-based simulation, which forgoes the calculation of the fluid flow and focuses on heat transfer and material insertion. This decision was based on past simulation development experience, where it was determined that the calculation of the fluid flow was the most computationally expensive part of the simulation.

The governing equations of the model developed can be seen in Equations 1, 2, and 3 which describe the flow of heat from conduction, convection and radiation, and laser absorption respectively [15].

$$\rho c_p \frac{\partial T}{\partial t} = k \left(\frac{\partial^2 T}{\partial x^2} + \frac{\partial^2 T}{\partial y^2} + \frac{\partial^2 T}{\partial z^2} \right) \quad (1)$$

$$k \frac{\partial T}{\partial n} = -h(T_s - T_a) - \epsilon \sigma (T_s^4 - T_a^4) + \phi(x, y, z) + \rho c \frac{\partial T}{\partial t} \quad (2)$$

$$\phi(x, y, z) = H(z) \alpha \phi_0 \sqrt{1 - \frac{x^2}{r_0^2} - \frac{y^2}{r_0^2}} \quad (3)$$

In these equations, ρ is density, c_p is specific heat, k is thermal conductivity, h is convection coefficient, ε is emissivity, σ is Stefan-Boltzmann constant, n is the unit (outward) normal vector of a point at location (x,y,z) that is located on the outer surface of the component, r_0 is the radius of the laser beam, α is the absorption of the material with respect to the laser radiation, T_s is the surface temperature, T_a is the ambient temperature, ϕ_0 is the laser power, and $H(z)$ is a step function which is 1 for the node with the largest z value in every (x, y) location and 0 elsewhere.

The main attributes of the model are its ability to predict the thermal history of a part, Figure 1a, the phase map of the part at any given time, Figure 1b, and a cooling rate for any section of the part, Figure 1c. This helps to give a predictor of the microstructure within the deposition which is the driving force behind the final mechanical properties. Additionally, the laser in the simulation is modeled in 3-D to be able to take into account

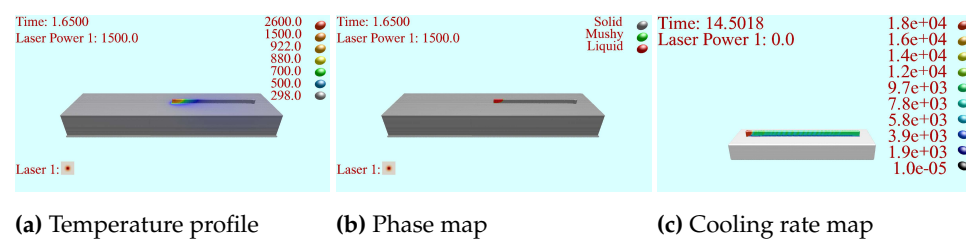


Figure 1. Examples of data maps which can be expected from the simulation.

the beam quality using the beam parameter product (BPP) reported by the manufacturer and shown in Equation 4, where θ and w_0 are the divergence angle and the beam waist respectively.

$$BPP = 0.5\theta w_0 \quad (4)$$

Lastly, the model includes true ray tracing enabling shadowing of the laser, the ability to define a mass which represents the machine acting as a heat sink during the build process, and the inclusion of temperature-dependent material properties.

The main objective of the model is to accurately predict the thermal history of the build. In order to initially validate the models, the well-characterized and published material of Ti-64 was used. The validation was done by scanning a laser on the surface of a substrate at three energy densities with the experimental parameters found in Table 1 and the material properties used in the simulations can be seen in Table 2.

Table 1. Simulation parameters used in Ti-64 validation

Parameter	Value
Resolution	60 μm
Laser diameter	2.0 mm
Laser Profile	TEM00
Laser power	1000 W
Energy density (Equation ??)	13, 18, 24 $\frac{W}{mm^3/sec}$
Scan Length	45 mm
Substrate dimensions	55 mm x 12.7 mm x 6.35 mm

There are several representations of the energy density of a laser beam in AM but the most appropriate method of calculating the energy for the DED process is to use a surface energy density, Equation 5, where P is laser power, A is the laser spot area, and v is the scan speed [17].

$$SED_{area} = \frac{P}{Av} \quad (5)$$

In order to analyze the results, the samples from the three parameter sets were sectioned, polished, and etched to make the melt track visible as can be seen in Figure 2a, this was done at three points along the melt length. The experiment and simulation were

Table 2. Ti-64 material properties used in validation

Material Property	Reference
Solidus temperature	[5]
Liquidus temperature	[16]
Solid density	[16]
Fluid density	[16]
Specific heat	[6]
Thermal conductivity	[6]
Absorptivity	[7]

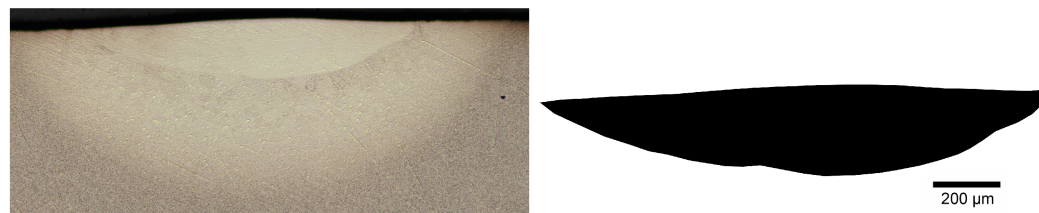


Figure 2. Analysis of sliced sample in Ti-64 validation

compared and the resulting error for the width can be seen in Figure 3a and the depth can be seen in Figure 3b. The average values which are reported on the graph have an associated

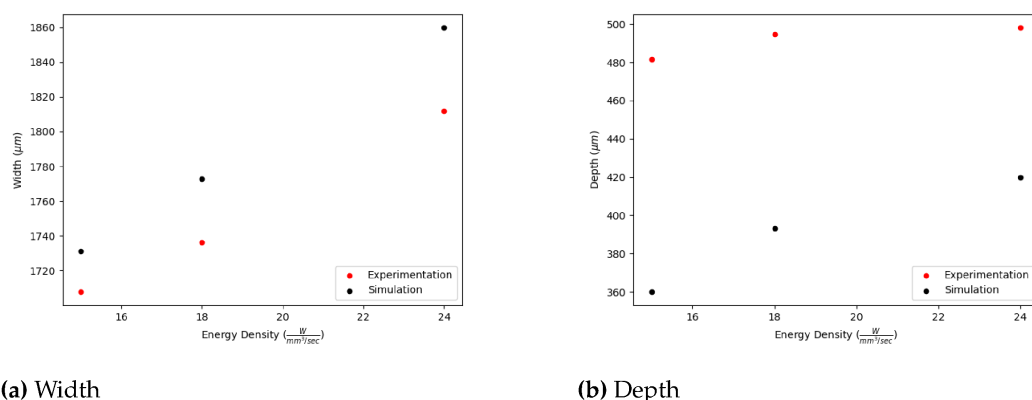


Figure 3. Comparison of simulation and experimentation in Ti-64 validation.

standard deviation of the $0.62 \mu m$, $13.7 \mu m$, and $7.74 \mu m$ for the width measurements for the energy densities of $15 \frac{W}{mm^3/sec}$, $18 \frac{W}{mm^3/sec}$, and $24 \frac{W}{mm^3/sec}$ respectively. For the track depth the standard deviations are $70.2 \mu m$, $113.7 \mu m$, and $13.7 \mu m$ for the energy densities of $15 \frac{W}{mm^3/sec}$, $18 \frac{W}{mm^3/sec}$, and $24 \frac{W}{mm^3/sec}$ respectively.

From the plots, it can be seen that the simulation is capable of predicting the width within 3% error and the depth error is between 15% and 25%. The error in the width is very acceptable at less than 3%. However, the error in the depth is larger due to the resolution (voxel size) of the simulation chosen and its relative size to the depth. This error, of approximately 20%, for the depths which range from 450-500 μm is 1.3-1.7 times the resolution, 60 μm , of the simulation. Since the trends of the simulation and experimentation match and the error is within two resolution distances the 20% error in the depth is considered acceptable as well. This shows that the mathematical models developed are accurate and if the material property is well characterized, the simulation will produce accurate results.

2.2. Tuning algorithm description

The search algorithm chosen was the Nelder-Mead search algorithm [18]. This method was selected because it is one of the most popular direct search methods for the minimiza-

tion of functions. The Nelder-Mead approach is a local optimization search which does not rely on knowledge of the gradient to select the next search point. This is critical for the application to simulation results because the gradient is unknown and finding it would involve running a large number of simulations. With simulation times that can reach into days long, this is a critical consideration. Instead of knowing the actual function, it relies on $n+1$ vertices. This results in a smaller number of simulation runs being needed to perform the minimization [19]. The flow chart in Figure 4 is the flow which is used to determine the next search point.

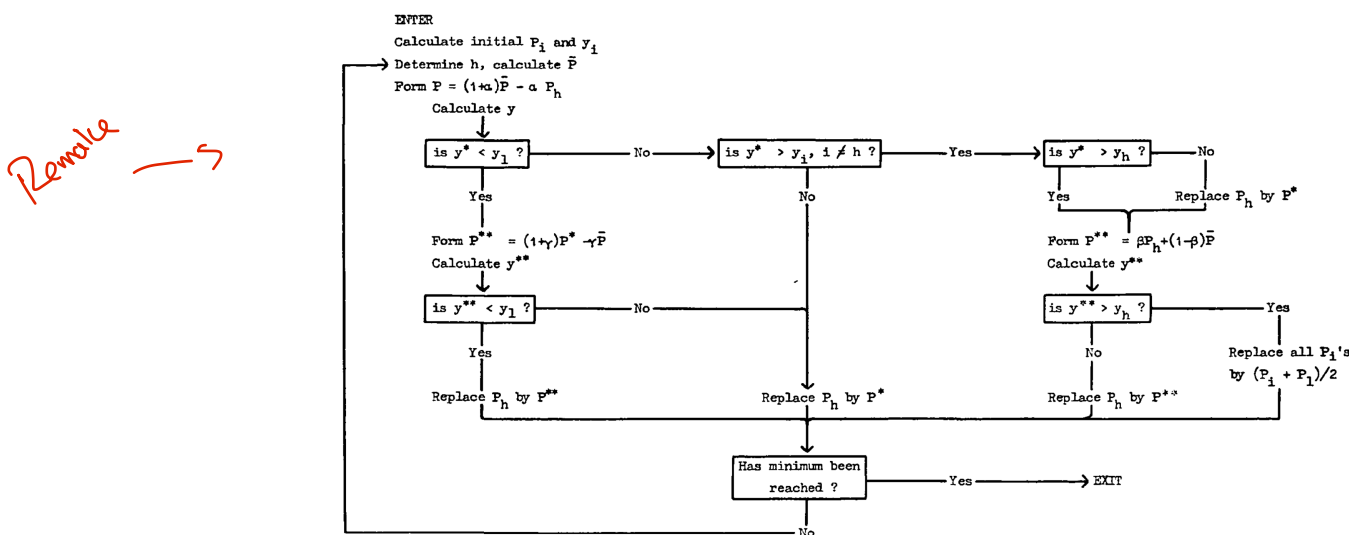


Figure 4. Flow chart for the Nelder-Mead search algorithm X

The search begins by calculating the reflection point using Equation 6 where α is the reflection coefficient.

$$P_{refl} = (1 + \alpha)P_{cent} - \alpha P_{high} \quad (6)$$

If this reflection point is smaller than the smallest current simplex value, then the expansion is calculated using Equation 7, where γ is the expansion coefficient.

$$P_{exp} = \gamma P_{refl} - (1 - \gamma)P_{center} \quad (7)$$

If the expansion point is smaller than the reflection point, then the expansion point is used to replace the largest simplex member. Otherwise, if the reflection point is larger than the expansion point, the reflection point is used to replace the largest member of the simplex, and the algorithm is restarted. If the reflection point is larger than the smallest simplex point and smaller than the second largest point, then the highest point of the simplex is replaced with the reflection and the algorithm is restarted. If the reflection point is between the simplex highest value and second highest value, a contraction is calculated, using Equation 6, with the highest values being replaced with the reflection. Otherwise the contraction is calculated with the original simplex still using Equation 6, where β is the contraction coefficient.

$$P_{cont} = \beta P_{high} - (1 - \beta)P_{cent} \quad (8)$$

If the contraction point is smaller than the largest point of the simplex, then the contraction replaces the largest point and the algorithm is continued. However, if the contraction point is larger than the highest point, a shrink step is performed, detailed in Equation 9, where δ is the shrink coefficient and the algorithm is restarted.

$$P_i = \delta P_i + (1 - \delta)P_{low} \quad (9)$$

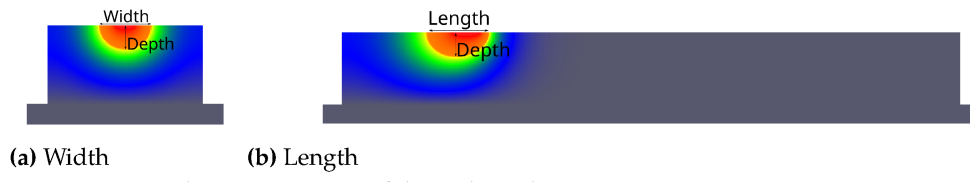


Figure 5. Example measurements of the melt pool

2.3. Selection of Properties

One of the attractive characteristics of the Nelder-Mead search algorithm is its ability to scale to an unlimited number of unknowns. The main adverse effects of the scaling are the increased number of runs and the combination of the errors. As the number of unknowns increases the complexity of the search space increases, which in turn increases the number of iterations needed to find a minimum. This can result in drastically longer wait times for the search results. Additionally, with the increased number of unknowns, the stop condition of the search algorithm will be met at a different interval since the stop condition is based on the variance in the simplex. This may result in modifications to the stop conditions being necessary as a larger number of unknowns are included. If the response variable is properly defined, it will not affect the model's results if more unknowns are included [19].

In order to reduce the complexity of the search algorithm, a sensitivity analysis was performed. This work began by finding the material properties which were needed in the models as summarized in Table 3.

Table 3. Key material properties in thermal modeling of AM

Material Property	Reference
Solidus temperature	[20], [8], [21], [22]
Liquidus temperature	[20], [8], [21], [22]
Solid density	[22], [23]
Fluid density	[22], [24], [9]
Specific heat	[8], [9]
Thermal conductivity	[8], [9]
Absorptivity	[25], [26], [27]

These properties were varied according to a Placket-Burman design of experiment in order to determine the properties which, when changed, had a statically significant effect on the resulting melt pool width, depth, and volume, as measured in Figure 5. Analyzing these results with Pareto charts of the standardized effects of the variables and partial regression plots of the residuals it was determined that the variables in Table 4 had a statically significant effect on the resulting melt track when modified. This work included

Table 4. Critical material properties

Laser absorption at 880°C
Laser absorption at 922°C
Thermal conductivity at 922°C
Thermal conductivity at 1491°C
Specific heat at 733°C

the laser diameter in the search algorithms dataset due to the difficulty associated with accurately measuring the diameter.

2.4. Tuning and Simulation setup

For this study, the Nelder-Mead search algorithm parameters which were used can be seen in Table 5. These parameters were chosen because they fell within the guidelines from

Table 5. Nelder-Mead algorithm parameters

Parameter	Value
α	5.0
γ	10.0
β	0.5
σ	0.5

the algorithm description and after trial and error produced the most efficient tuning [18].

The starting values which were used as the starting point for the search algorithm can be seen in Table 6. These values were chosen based on the values which were found in the literature for similar aluminum alloys. The laser diameter was chosen based on the measuring of a melt track width on a substrate. To ensure the search algorithm did not

Table 6. Material properties found in the literature

Property	Material Temp.	Value	Ref.
Laser absorption	880°C	15.0%	[26]
Laser absorption	922°C	30.0%	[26]
Thermal conductivity	922°C	88.8 $\frac{W}{mK}$	[9]
Thermal conductivity	1491°C	104.9 $\frac{W}{mK}$	[9]
Specific heat	733°C	1108.0 $\frac{J}{kgK}$	[9]
Laser diameter		1.6 mm	

waste time searching in unacceptable regions the constraint was included that none of the material properties were allowed to become negative. This was the only constraint which was needed in addition to the inherent constraints of the Nelder-Mead algorithm.

The experimental setup which was used was a simple laser scanning of the surface of a substrate, as shown in Figure 6, with the parameters shown in Table 7. This was chosen in order to simplify the experiment. This setup removes the complexity associated with adding material which includes the rate of material addition, molten metal flow parameters, and acceleration effect associated with turning during deposits.

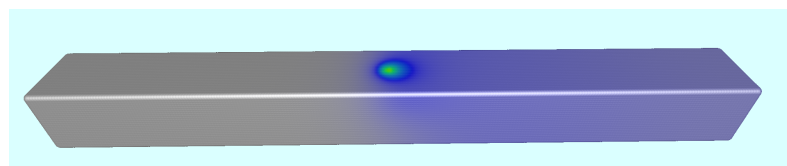


Figure 6. Example of simulation setup used to determine melt track size

Table 7. Experimental constants used in tuning experiments

Parameter	Value
Resolution (voxel size)	100 μm
Laser Power	1,750 W
Laser Scan Speed	1143 mm/min
Laser Profile	Top Hat
Scan Length	77 mm
Substrate dimensions	82 mm x 8 mm x 8 mm

179

180

181

182

183

184

185

186

187

188

189

190

191

192

193

194

2.5. Simulation analysis

Upon completion of each simulation run, the saved data files were analyzed to determine the regions of the simulation which had melted. This was done by developing a map which marked the locations of the domain that had ever been in the fluid phase. This map was then used to determine the width and depth of the melt track along the scan length, excluding the beginning and end where effects from starting and stopping motion would affect the results. These width and depth measurements along the scan length were averaged to develop a single measurement which could be compared to experimentation.

The experimental results were similarly determined, however instead of a continuous set of measurements, there were 4 discrete measurements. These were obtained by slicing the substrate at the prescribed locations using a wire electrical discharge machine (EDM). These slices were polished and etched in order to make the microstructural differences visible, an example of this can be seen in Figure 7, where the dark region had been melted during the experimentation.

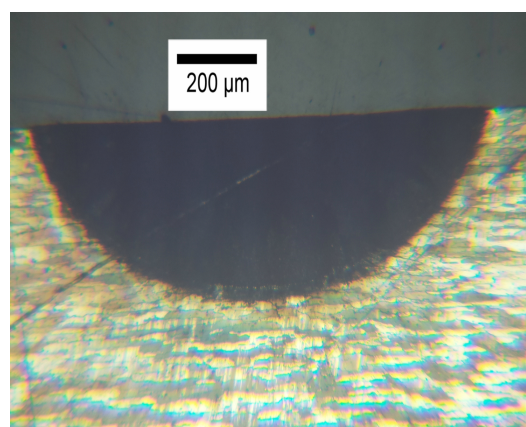


Figure 7. Example of sliced, polished, and etched slice from experimentation

In order for the Nelder-Mead search to function properly, a response variable needed to be defined. This function needed to characterize the accuracy of the simulation into a single parameter which could be minimized and upon minimization would result in the most accurate simulation. To accomplish this goal, Equation 10 was developed. This equation takes into account the error in the width of the simulation along with the error in the depth. This equation results in a non-negative number where 0 represents a simulation which perfectly matched experimentation.

$$\text{Response} = \left(\frac{| \text{Sim. Width} - \text{Exp. Width} |}{\text{Exp. Width}} + \frac{| \text{Sim. Depth} - \text{Exp. Depth} |}{\text{Exp. Depth}} \right) * 100 \quad (10)$$

3. Results

3.1. Search algorithm results

The search algorithm was allowed to search the space to determine the best material properties. The resulting response variables can be found in Figure 8. Where the blue circular markers indicate material datasets which developed a melt track and the red diamond markers did not have the energy density to produce a melt track. Due to the vast difference in scales of the initial responses and the final response variables, a new plot was created which has a max Y value of just over 30. In this plot the blue circular markers are ones which have a response variable less than 30, the green triangle markers are those which completed with a melt track but had response variables greater than 30, and the red

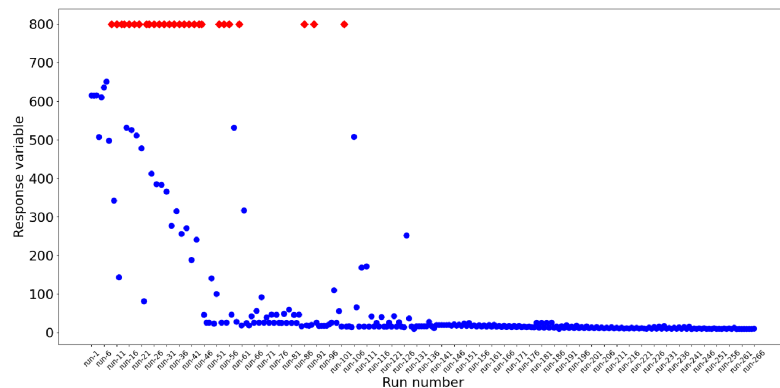


Figure 8. Response variable of the search algorithm for material properties and laser diameter

diamond markers are those which did not produce a melt track. In addition to these plots,

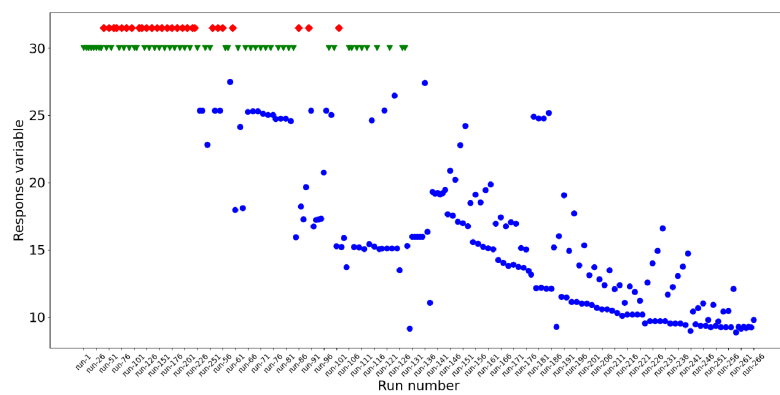
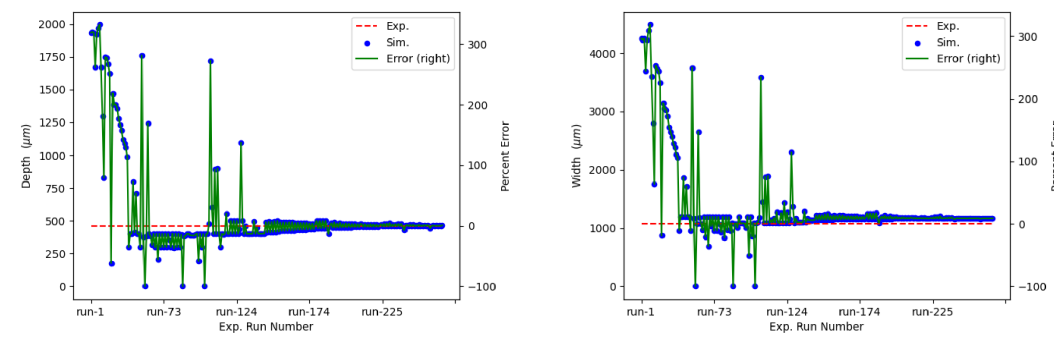


Figure 9. Response variable of the search algorithm for material properties and laser diameter with max y axis value of 30

the error in the width and depth were plotted and can be seen in Figure 10. In these plots, it can be seen that the error in the width is 8.83% and the error in the depth is 0.03%. It is not fully understood why all the error is coming from the width, however, it is theorized that this is a product of the difference in the size of the width vs the depth since the width is nearly triple that of the depth.



(a) Melt track depth

(b) Melt track width

Figure 10. Error in the individual runs of the simulations during the tuning algorithm

The search algorithm completed and reduced the combined error from over 600% when starting from the material properties found in the literature for the generic aluminum material properties, found in Table 6, to 9.1% when using the values found in Table 8.

226
227
228
229
230

231
232
233
234

Table 8. Optimized material properties and laser diameter dataset for the developed simulation

Property	Material Temp.	Value
Laser absorption	880°C	16.8%
Laser absorption	922°C	10.0%
Thermal conductivity	922°C	32.2 $\frac{W}{mK}$
Thermal conductivity	1491°C	152.3 $\frac{W}{mK}$
Specific heat	733°C	2957.6 J/kgK
Laser diameter		0.864 mm

3.2. Search results validation

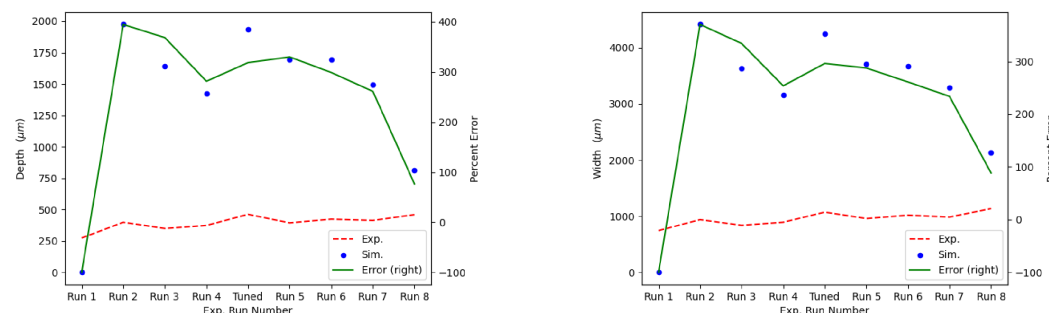
In order to ensure that the search algorithm results were valid across laser travel speeds and power levels, a range of 8 other parameters were compared with experimental results. These experiments and simulations were the setup and analyzed as was used for the tuning experimental setup. The base experimental parameters can be seen in Table 7 with the scan speed and laser power being varied as seen in Table 9 and the simulation material properties were used from Table 8. The experimental result were collected and

Table 9. Validation processing parameters

Exp. Id.	Scan speed (mm/min)	Laser Power (W)
1	762	1000
2	762	1500
3	762	1250
4	1143	1250
5	1143	1500
6	1524	1750
7	1524	1500
8	1524	2000

graphed in Figure 12 and 11 as the red dashed line and were used as the ground truth with which the models were compared.

These speeds and powers were first completed with the literature determined values from Table 6 and the results can be seen in Figure 11. Where the red dashed line is the



(a) Melt track depth

(b) Melt track width

Figure 11. Comparison of experimental and simulated results for validation points with generic literature values for material dataset

experimental results, the blue dots are the simulation predictions, and the green line is the error when comparing the simulated results to the experimental results. These results show that over the 9 initial parameter sets, when a melt track was developed, the average absolute value of the error in the depth was approximately 290% and the average error in the width was approximately 265%. To put this into terms of the response variable of

the search algorithm, the sum of the width and depth error, would be 555% combined error. Additionally, run 1 was unable to develop a melt pool, which is contrary to the experiments where all the parameter sets had a stable melt track. These results corroborate the results from Figure 8 which showed that the parameter set used for tuning initial dataset of material properties found in the literature is wholly inadequate for simulating the process at hand.

In contrast to these results, the material dataset which was found in Table 8 was used to simulate each parameter set, and the results can be seen in Figure 12. Where the

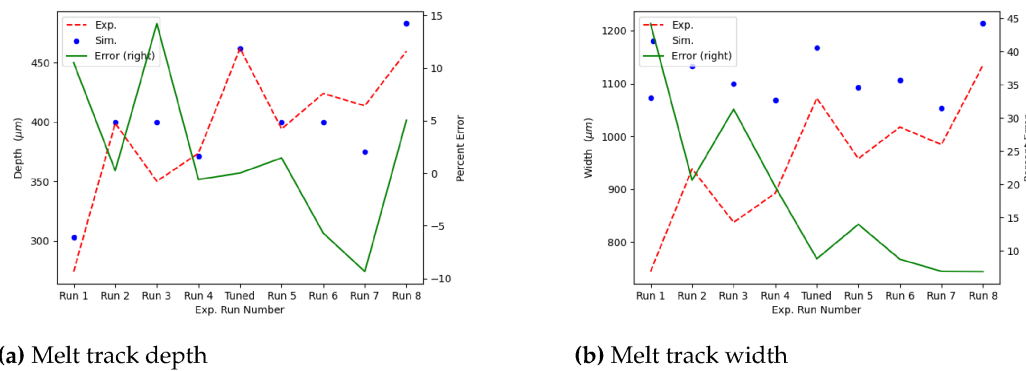


Figure 12. Comparison of experimental and simulated results for validation points with optimized values for material dataset

red dashed line is the experimental results, the blue dots are the simulation predictions, and the green line is the error when comparing the simulated results to the experimental results. These results show the average error in the width was approximately 17% and the average error in the depth was approximately 5%, which creates a combined error of only 22%. These results show that the optimized dataset is better at predicting the combined error of the simulation by over 500%. This results in a simulation which can be leveraged more intensely during the process development and build qualification process. These results are from a wide parameter set which encompasses most of the usable parameter space for deposition found experimentally. This improvement in accuracy will allow for a greater application in the model in the determination of an optimized parameter set for a given build. In addition, the model is seen to be more accurate at parameters above the parameter used during the optimization. This leads to the conclusion that if a more accurate simulation is needed, the optimization should be done at a parameter set near the desired parameter set.

4. Discussion

This work shows that the Nelder-Mead search algorithm is an appropriate multidimensional search algorithm for the determination of the optimal dataset for improved simulation accuracy. It was capable of reducing the simulated melt track depth and width of a set of processing parameters by over 500%, as shown in Figures 11 and Figure 12, which used datasets from literature (Table 6) and the optimized dataset (Table 8) respectively. This was done by defining the response variable (Equation 10) for the search algorithm to be the sum of the error in the width and the depth, which facilitated an efficient search. This methodology can be used to develop accurate simulations for any material which is not well published or to increase the accuracy of a simulation which utilizes approximations of first principles in order to increase its efficiency.

Author Contributions: Conceptualization, Aaron Flood and Frank Liou; methodology, Aaron Flood and Frank Liou; software, Aaron Flood; validation, Aaron Flood and Rachel Boillat; formal analysis, Aaron Flood; investigation, Aaron Flood, Rachel Boillat, and Sriram Isanaka; resources, Frank Liou; data curation, Aaron Flood and Rachel Boillat; writing—original draft preparation, Aaron Flood and

Frank Liou; writing—review and editing, Aaron Flood and Frank Liou; visualization, Aaron Flood; supervision, Sriram Isanaka and Frank Liou; project administration, Frank Liou; funding acquisition, Frank Liou. All authors have read and agreed to the published version of the manuscript.

Funding: This research was partially funded by the National Science Foundation Grants CMMI 1625736 and EEC 1937128, Intelligent Systems Center and Material Research Center at Missouri S&T. Their financial support is greatly appreciated.

Data Availability Statement: All data generated or analyzed during this study are included in this published article.

Conflicts of Interest: The authors declare no conflict of interest.

References

1. Wang, D.; Chen, X. Closed-Loop High-Fidelity Simulation Integrating Finite Element Modeling With Feedback Controls in Additive Manufacturing. *Journal of Dynamic Systems, Measurement, and Control* **2021**, *143*, 021006. <https://doi.org/10.1115/1.4048364>.
2. Roy, M.; Wodo, O. Data-Driven Modeling of Thermal History in Additive Manufacturing. *Additive Manufacturing* **2020**, *32*, 101017. <https://doi.org/10.1016/j.addma.2019.101017>.
3. Moges, T.; Yang, Z.; Jones, K.; Feng, S.; Witherell, P.; Lu, Y. HYBRID MODELING APPROACH FOR MELT POOL PREDICTION IN LASER POWDER BED FUSION ADDITIVE MANUFACTURING **2020**. p. 15.
4. Daryabeigi, K. Thermal Properties for Accurate Thermal Modeling, 2011.
5. Welsch, G.; Boyer, R.; Collings, E. *Materials Properties Handbook: Titanium Alloys*; ASM international, 1993.
6. Boivineau, M.; Cagran, C.; Doytier, D.; Eyraud, V.; Nadal, M.H.; Wilthan, B.; Pottlacher, G. Thermophysical Properties of Solid and Liquid Ti-6Al-4V (TA6V) Alloy. *International Journal of Thermophysics* **2006**, *27*, 507–529. <https://doi.org/10.1007/PL00021868>.
7. Fan, Z.; Liou, F. Numerical Modeling of the Additive Manufacturing (AM) Processes of Titanium Alloy. In *Titanium Alloys - Towards Achieving Enhanced Properties for Diversified Applications*; Amin, A.N., Ed.; InTech, 2012. <https://doi.org/10.5772/34848>.
8. Lundberg, S. *Material Aspects of Fire Design*, 1994.
9. Leitner, M.; Leitner, T.; Schmon, A.; Aziz, K.; Pottlacher, G. Thermophysical Properties of Liquid Aluminum. *Metallurgical and Materials Transactions A* **2017**, *48*, 3036–3045. <https://doi.org/10.1007/s11661-017-4053-6>.
10. JMatPro. <https://www.sentesoftware.co.uk/jmatpro>.
11. Qi, Y. A High Strength Al-Li Alloy Produced by Laser Powder Bed Fusion_ Densification, Microstructure, and Mechanical Properties. *Additive Manufacturing* **2020**, p. 10.
12. Weiss, D. Improved High-Temperature Aluminum Alloys Containing Cerium. *Journal of Materials Engineering and Performance* **2019**, *28*, 1903–1908. <https://doi.org/10.1007/s11665-019-3884-2>.
13. Weiss, D. Developments in Aluminum-Scandium-Ceramic and Aluminum-Scandium-Cerium Alloys. In *Light Metals 2019*; Chesonis, C., Ed.; Springer International Publishing: Cham, 2019; pp. 1439–1443. https://doi.org/10.1007/978-3-030-05864-7_18.
14. Singh, A. Additive Manufacturing Of Al 4047 And Al 7050 Alloys Using Direct Laser Metal Deposition Process. PhD thesis, 2017.
15. Han, J.C. *Analytical Heat Transfer*; CRC Press, 2012.
16. Mills, K. Recommended Values of Thermophysical Properties for Selected Commercial Alloys. In *Recommended Values of Thermophysical Properties for Selected Commercial Alloys*; Woodhead Publishing Series in Metals and Surface Engineering, Woodhead Publishing, 2002; pp. 211–217.
17. Kurzynowski, T.; Stopryra, W.; Gruber, K.; Ziolkowski, G.; Kuźnicka, B.; Chlebus, E. Effect of Scanning and Support Strategies on Relative Density of SLM-ed H13 Steel in Relation to Specimen Size. *Materials* **2019**, *12*, 239. <https://doi.org/10.3390/ma12020239>.
18. Nelder, J.A.; Mead, R. A Simplex Method for Function Minimization. *The Computer Journal* **1965**, *7*, 308–313. <https://doi.org/10.1093/comjnl/7.4.308>.
19. Wang, P.C.; Shoup, T.E. Parameter Sensitivity Study of the Nelder–Mead Simplex Method. *Advances in Engineering Software* **2011**, *42*, 529–533. <https://doi.org/10.1016/j.advengsoft.2011.04.004>.
20. Joseph R. Davis. Aluminum and Aluminum Alloys Davis. In *Alloying: Understanding the Basics*; ASM International, 2001.
21. Ulrich. 6000 & 7000 Series Aluminum Alloy, 2014.
22. ASM. Aluminum 6061-T6; 6061-T651. <http://asm.matweb.com/search/SpecificMaterial.asp?bassnum=MA6061T6>, 2022.
23. AmesWeb. ALUMINUM 6061 MATERIAL PROPERTIES. <https://amesweb.info/Materials/Aluminum-6061-Properties.aspx>, 2022.
24. Schmitz, J.; Hallstedt, B.; Brillo, J.; Egry, I.; Schick, M. Density and Thermal Expansion of Liquid Al–Si Alloys. *Journal of Materials Science* **2012**, *47*, 3706–3712. <https://doi.org/10.1007/s10853-011-6219-8>.
25. Funck, K.; Nett, R.; Ostendorf, A. Tailored Beam Shaping for Laser Spot Joining of Highly Conductive Thin Foils. *Physics Procedia* **2014**, *56*, 750–758. <https://doi.org/10.1016/j.phpro.2014.08.082>.
26. Boyden, S.B.; Zhang, Y. Temperature and Wavelength-Dependent Spectral Absorptivities of Metallic Materials in the Infrared. *Journal of Thermophysics and Heat Transfer* **2006**, *20*, 9–15. <https://doi.org/10.2514/1.15518>.

27. El-Hameed, A.M.A.; Abdel-Aziz, Y.A.; El-Tokhy, F.S. Anodic Coating Characteristics of Different Aluminum Alloys for Spacecraft Materials Applications. *Materials Sciences and Applications* **2017**, *08*, 197–208. <https://doi.org/10.4236/msa.2017.82013>. 344
345

Disclaimer/Publisher's Note: The statements, opinions and data contained in all publications are solely those of the individual author(s) and contributor(s) and not of MDPI and/or the editor(s). MDPI and/or the editor(s) disclaim responsibility for any injury to people or property resulting from any ideas, methods, instructions or products referred to in the content. 346
347
348